Stimulation of heterotrophic and autotrophic metabolism in the mixing zone of the Kuroshio Current and northern South China Sea: implications for export production

Yibin Huang[1,2], Edward Laws[3], Bingzhang Chen[4], Bangqin Huang*[1,2]

[1]State Key Laboratory of Marine Environmental Science, Xiamen University, Xiamen, China.

[2]Fujian Provincial Key Laboratory of Coastal Ecology and Environmental Studies, Xiamen University, Xiamen, China.

[3]Department of Environmental Sciences, College of the Coast and Environment, Louisiana State University, Baton Rouge, Louisiana, USA.

[4]Department of Mathematics and Statistics, University of Strathclyde, Glasgow, United Kingdom.

Correspondence to: Bangqin Huang, bqhuang@xmu.edu.cn

Key points:

- A field investigation of the impact of Kuroshio Current on the microbial metabolism in the oligotrophic northern South China Sea basin
- Increases heterotrophic bacterial activity and primary production were associated with the Kuroshio Current intrusion
- A shift of metabolic status from the net heterotrophy to the prevailing autotrophy was observed in the mixing zone

Abstract

To evaluate the influences of the Kuroshio Current intrusion on the biogeochemistry of the northern South China Sea (NSCS), we conducted field observations of the responses of microbial metabolism to the intrusions of the Kuroshio Current into the NSCS. We used an isopycnal mixing model to quantitatively assess the extent of the Kuroshio intrusion into the NSCS and found that bacterial abundance, production, and growth efficiency were unimodal functions of the fraction of Kuroshio water. Values were maximal at ~60% Kuroshio water and decreased monotonically as the percent of Kuroshio water deviated from 60%. The patterns of gross primary production and nitrate concentration were similar, but the peaks occurred at ~50% Kuroshio water. The Kuroshio intrusion, however, had little impact on bacterial and community respiration. The observed elevation of nitrate concentrations at ~50% Kuroshio water was quantitatively consistent with estimates of the amount of inorganic nitrogen released by remineralization of dissolved organic nitrogen by bacteria. Based on these observations, we hypothesize that dissolved organic matter (DOM) in the Kuroshio water stimulates bacterial activity, and catabolism of the DOM releases inorganic nutrients that stimulate primary production in the NSCS basin. The concomitant elevation of net community production subsequently enhances export production and thereby strengthens the biological pump in the nitrogen-limited NSCS basin. Recognition of this mechanism underscores the role of horizontal currents in regional carbon and nitrogen cycles and broadens

understanding of the processes that sustain export production in the oligotrophic ocean.

Plain Langue Summary

Horizontal currents universally occur in the global ocean, however, the knowledge of associated impacts in the biogeochemical processes is still poorly represented. We firstly estimate the degree of horizontal Kuroshio Current in the different sampling stations in the oligotrophic regime of northern South China Basin. Then we found the significant increase of autotrophic primary production, heterotrophic bacterial abundance, and bacterial production in the regions with a moderate fraction of Kuroshio water. Such changes led to higher net community production. We further linked the observations of changes in nutrient pools with the microbial activities to figure out a more comprehensive picture of the impact of the Kuroshio current in biogeochemical processes in the northern South China Basin. As the ocean is toward greater processes relative to the vertical processes due to more stratification in the upper water, our study is also a step forward understanding the potential feedbacks of marine to the climate change.

Keywords: Microbial metabolism, Bacteria, Net community production, Kuroshio Current intrusion, Northern South China Sea

1. Introduction

Nearly half of the primary production on Earth occurs in the ocean [*Falkowski et al.*, 2003], and plankton-mediated carbon transfer from the atmosphere into the ocean interior, namely the "soft-tissue biological pump", plays a critical role in regulating atmospheric CO_2 levels on geological timescales [*Siegel et al.*, 2014; *Sigman and Boyle*, 2000]. Photosynthesis captures CO_2 from the atmosphere and provides most of the organic carbon for aquatic heterotrophs, whereas heterotrophic activity subsequently releases the carbon back into the atmosphere as CO_2. Among the various heterotrophs, bacteria consume a large amount of the organic carbon [*P A del Giorgio et al.*, 1997] and play a fundamental role in recycling through the microbial loop [*Azam et al.*, 1983; *Ducklow*, 1999]. The magnitude of microbial metabolism in the upper water column is therefore an important determinant of the efficiency of oceanic CO_2 uptake and ocean-atmosphere coupling within the climate system.

In the oligotrophic ocean, the largest biome on Earth, current understanding of the mechanism that controls microbial activity has focused mainly on proximate factors (i.e., light, nutrients, and community structure) and associated temporal variability [*Gist et al.*, 2009; *Jenkins and Doney*, 2003; *Viviani and Church*, 2017]. However, recent observations have indicated that proximate factors are insufficient to explain the observed biogeochemical variability with depth, even in the central gyres [*Johnson et al.*, 2010; *Lozier et al.*, 2011]. This inadequacy has led to more attention's being paid to the potential influence of horizontal currents. Previous studies have been

focused mainly on elucidating hydrographic changes and physical dynamics [*Hu et al.*, 2015; *Huthnance et al.*, 2009]. The impacts of currents on biogeochemical processes have received relatively little attention [*Abell et al.*, 2000; *Fontes et al.*, 2018; *Reynolds et al.*, 2014]. Based on a global circulation model, *Letscher et al.* [2016] have demonstrated that organic matter transported by currents could account for a considerable fraction of export production in the oligotrophic ocean and as much as 24–36% of nitrogen export and 40–67% of phosphorus export on a global scale. The inorganic nutrients transported by horizontal currents have been observed to be rapidly consumed near gyre margins, but the transport of organic matter is commonly assumed to precede remineralization of the organic matter into inorganic compounds [*Bronk et al.*, 2007; *Letscher et al.*, 2016]. The mechanism of how currents contribute to the biogeochemical cycling of carbon remains unclear because of the paucity of field investigations of biogeochemical responses to horizontal advection and mixing.

The South China Sea is the world's largest marginal sea in the western Pacific Ocean. The northern South China Sea (NSCS) basin during the warm season is typically a nitrogen-limited ecosystem. It is characterized by low nitrate concentrations, primary production, and export production [*Liu et al.*, 2002; *Ning et al.*, 2004] because of strong stratification in the upper water column [*Wong et al.*, 2007] and relatively little nitrogen fixation [*Lee Chen et al.*, 2008]. However, the NSCS basin is characterized by dynamic interactions with the adjacent Pacific Ocean through the Luzon Strait [*Dai et al.*, 2013; *Nan et al.*, 2015]. The Kuroshio Current,

111 the western boundary current of the North Pacific subtropical gyre, flows from
112 roughly 15° to 35° north latitude [*Hu et al.*, 2015]. Over the course of one year, the
113 Kuroshio Current frequently intrudes into the NSCS via the Luzon Strait. The vertical
114 distribution of the currents through the strait mimics a sandwich structure: water
115 enters the NSCS at depths of 0–400 m and ~1500–3000 m, and it returns to the
116 western Pacific Ocean at intermediate depths of ~500–1500 m [*Dai et al.*, 2013; *Nan*
117 *et al.*, 2015; *Qu et al.*, 2000]. The Kuroshio Current is typically characterized by
118 warmer and more saline water but extremely low nutrient concentrations relative to
119 the NSCS [*Du et al.*, 2013]. The relatively deep nitracline of the Kuroshio favors the
120 growth of *Trichodesmium* and high N_2 fixation rates [*Lee Chen et al.*, 2008; *Shiozaki*
121 *et al.*, 2015]. The Kuroshio, although oligotrophic, has been reported to have higher
122 dissolved organic carbon (DOC) concentrations (60–79 mmol m^{-3}) than the NSCS
123 (51–70 mmol m^{-3}) based on seasonal observations in this region [*Wu et al.*, 2015].
124 The unique characteristics of the Kuroshio Current and its frequent interactions with
125 the NSCS basin thus provide an ideal laboratory for studying the effects of currents
126 on biogeochemical processes in the oligotrophic ocean. Here, using data collected
127 from a research cruise in the NSCS basin during a period when a significant Kuroshio
128 intrusion was detected [*Xu et al.*, 2018], we used an isopycnal mixing model [*Du et*
129 *al.*, 2013] to quantify the proportion of water contributed by the Kuroshio in the upper
130 water column. Next, we analyzed concurrent measurements of autotrophic and
131 heterotrophic metabolism together with previously published observations of nutrient

pools during the same cruise to construct a more comprehensive picture of the impact of the Kuroshio Current on biogeochemical processes in the NSCS basin.

2. Methods

2. 1 Study sites

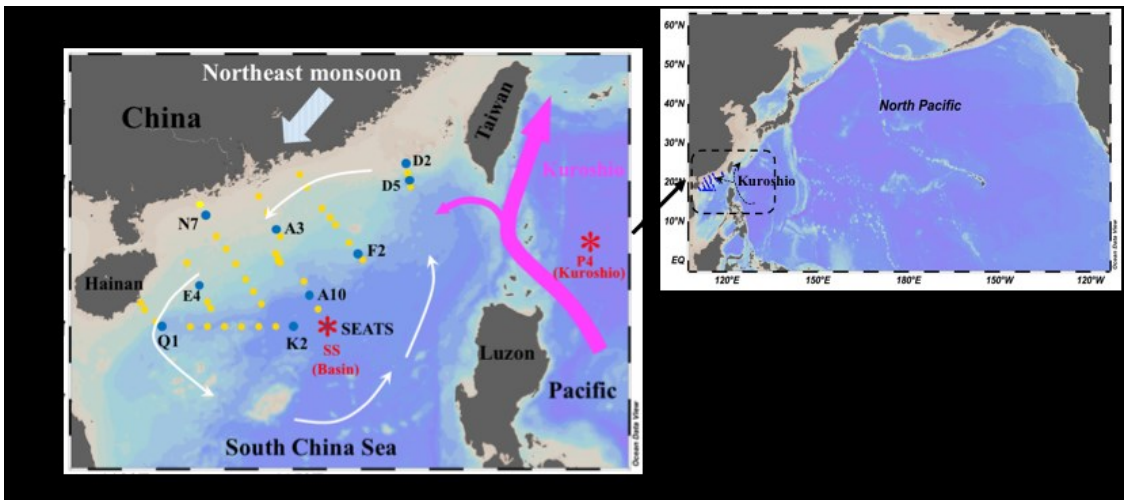

Figure 1. Map of the study area in the northern South China Sea (NSCS) from 15 May to 7 June 2016. The yellow and blue dots indicate sampling stations, at 10 of which (blue dots) incubation experiments were conducted. The white arrow represents the surface circulation in the NSCS during the northeast monsoon. The red and black stars indicate typical Kuroshio water (P4) and South China Sea water (SS), which were selected as the two end members for the isopycnal mixing model in accord with *Du et al.* [2013].

Our study area was located in the NSCS basin (Figure 1), which is effectively isolated from terrestrial inputs because of the seasonal changes of the basin-wide circulation gyre [*Hu et al.*, 2000]. During the summer, the NSCS basin is typically characterized by oligotrophic conditions, with low biomass and nutrient concentrations due to the extensive stratification that occurs in the upper water

column [*Gong et al.*, 2003; *Lee Chen and Chen*, 2006]. Recent studies have demonstrated that the intrusion of the Kuroshio Current into the NSCS significantly impacts the nutrient inventory, dissolved organic carbon pool, and nitrogen cycling in the upper 100 m of the water column [*Du et al.*, 2013; *Wu et al.*, 2015; *Xu et al.*, 2018].

2. 2 Chemical and biological assays

The research cruise was conducted from 15 May to 7 June 2016 onboard the R.V Dongfanghong II. Forty-eight stations were visited, including 10 stations for incubation experiments (Figure 1). Samples were collected with a 24-bottle Niskin rosette system with 12-L PVC bottles. Water temperature and salinity were measured with a conductivity-temperature-depth probe (SBE 911, Sea-Bird Electronics) attached to the rosette. For each sampling depth, ~50-ml water samples were collected for determination of nutrient concentrations and preserved at −20 °C until analysis. The concentrations of nitrate plus nitrite were measured with an AutoAnalyzer (Technicon AA3, Bran-Lube, GmbH) following the procedures described in *Han et al.* [2012]. For low-level NO_2^- and NO_3^- analyses, we used the flow injection analysis-liquid waveguide capillary cell method, which has a detection limit of 2 nmol L^{-1} [*Patey et al.*, 2008]. Ammonium concentrations were determined by the fluorometric o-phthaldialdehyde method with a detection limit of 0.7 nmol L^{-1} [*Zhu et*

al., 2013]. The chemical data from the same cruise have been published by *Xu et al.* [2018].

For the phytoplankton community structure, 4–5 liters of seawater from each depth were filtered onto 25-mm diameter GF/F filters under a low vacuum pressure (<40 mm Hg). The filters were stored in liquid nitrogen before the pigments were extracted with 2 mL of N,N-dimethylformamide (DMF) for 2 h in the dark at 2–8 °C. Phytoplankton pigment concentrations were measured by high-performance liquid chromatography (HPLC). The detailed analytical procedures for the HPLC analysis and pigment identification have been described by *Liu et al.* [2016]. The CHEMTAX program [*Mackey et al.*, 1996] was used to estimate the relative contributions of taxa to the total chlorophyll *a* (Chl-*a*) based on the pigment data. Thirteen diagnostic pigments were used to associate the fractions of the total Chl-*a* pool with nine phytoplankton groups: dinoflagellates (Dino), diatoms (Diat), haptophytes (Type 8) (Hapt_8), haptophytes (Type 6) (Hapt_6), chlorophytes (Chlo), cryptophytes (Cryp), *Prochlorococcus* (Proc), *Synechococcus* (Syne), and prasinophytes (Pras). The initial input ratios of the diagnostic pigments to Chl-*a* (Table S2) were based on ratios used in previous studies in the NSCS ([*Wang et al.*, 2016; *Xiao et al.*, 2018]).

For determination of bacterial abundance, 1.8-ml water samples were fixed with 1% (final concentration) seawater-buffered paraformaldehyde and stored at −80°C. The bacterial abundances were enumerated using an Accuri C6 flow cytometer (Becton, Dickinson, USA) after staining with 0.01% (final concentration) SYBR

Green (Molecular Probes) [*Marie et al.*, 1997]. Yellow-green latex beads (0.5 μm, Polysciences) were also added to the samples during the measurements as an internal standard.

2.3 The isopycnal mixing model

To quantify the impact of the Kuroshio intrusion on the NSCS basin, we adopted a well-validated, two-endmember isopycnal mixing model. The assumption behind the model was that mixing between the different water masses was dominated by isopycnal mixing, and diapycnal mixing was comparatively insignificant [*Du et al.*, 2013]. The detailed methodology and validation of this model were introduced by *Du et al.* [2013] and have been applied in recent studies [*Wu et al.*, 2015; *Xu et al.*, 2018]. Briefly, we chose two representative stations, P4 (123°E, 20°N) and SS (116°E, 18°N), to represent the Kuroshio and NSCS water endpoints, respectively, for the isopycnal mixing model (Figure 1). Based on the characteristics of the endmembers, the conservative equations in term of potential temperature (θ) or salinity (S) along the isopycnal plane can be expressed by Eq. 1 and Eq. 2:

$$R_{K\theta} + R_{S\theta} = 1 \quad \text{or} \quad R_{KS} + R_{SS} = 1 \qquad \text{Eq. 1}$$

$$R_{K\theta} \times \theta_K + R_{S\theta} \times \theta_S = \theta \quad \text{or} \quad R_{KS} \times S_K + R_{SS} \times S_S = S \qquad \text{Eq. 2}$$

where R_K and R_S are the fractions of Kuroshio water and NSCS water, respectively ($R_{K\theta}$ and R_{KS} represent the results derived from θ and S, respectively). The values of

θ_K and S_K indicate the endmember values of θ and S for the Kuroshio water, and θ_S and S_S represent the corresponding values for the NSCS. The contribution from the Kuroshio (R_K) endmember water can then be obtained as follows:

$$R_K = R_{K\theta} = (\theta - \theta_S) / (\theta_K - \theta_S) \quad \text{or} \quad R_K = R_{KS} = (S - S_S) / (S_K - S_S) \quad \text{Eq. 3}$$

In the present study, salinity (S) was selected as an indicator to estimate R_k at each sampling station in accord with the study of *Du et al.* [2013] because θ is likely affected by heat flux [*Qiu et al.*, 2015]. Although the upper intrusion of the Kuroshio into the NSCS may extend to a depth of 400 m [*Fang et al.*, 2009; *Tian et al.*, 2009], the R_K values reported here are the average fractions of Kuroshio water in the upper 100 m because most of the intense biological activity occurs in the euphotic zone, which usually extends to depths of 80–100 m in our study region [*Lee Chen*, 2005; *Tseng et al.*, 2005].

2.4 *In vitro* oxygen-based microbial metabolism

The first CTD cast before dawn was used to collect the water sample for the incubation experiment. Microbial metabolism was derived from the changes in dissolved oxygen concentrations during 24-h incubations [*Huang et al.*, 2019]. The dissolved oxygen concentration was determined by high-precision Winkler titration [*Oudot et al.*, 1988] with an automated potentiometric end-point detection system (Metrohm-848, Switzerland). This method achieves a precision of about 0.04%

231 (coefficient of variation) at oxygen concentrations between 70 and 250 mmol O_2 m^{-3}
232 [*Furuya and Harada*, 1995]. Samples from five discrete depths, corresponding to
233 100%, 50%, the deep chlorophyll maximum (DCM), 10%, and 1% of surface
234 irradiance (I_0) were collected at the incubation stations, where the depths of the water
235 column exceeded 200 m. If the depth of the DCM was coincident with the base of the
236 euphotic zone, additional depths between the depth corresponding to 10% light and
237 the DCM were collected. The water samples were siphoned into twelve calibrated
238 100-ml borosilicate bottles, and ~300 ml was allowed to overflow. The dissolved
239 oxygen in the four bottles was immediately fixed at the start of the incubation (initial
240 bottles). Two sets of four light and four dark incubation bottles were placed in a large
241 tank filled with water exposed to natural sunlight. The light bottles were covered with
242 neutral density meshes to adjust the light conditions to match the *in situ* irradiances at
243 the corresponding sampling depths. The incubation temperature was maintained by
244 running surface seawater. Gross primary production (GPP) was calculated as the
245 difference between the average dissolved oxygen concentrations in the light and dark
246 bottles after 24-h incubations; community respiration (CR) was equated to the
247 difference between the average dissolved oxygen concentrations in the initial and dark
248 bottles. The average propagated standard errors were 0.26 mmol O_2 m^{-3} d^{-1} for GPP
249 and 0.19 mmol O_2 m^{-3} d^{-1} for CR (n = 50). NCP was defined as the difference
250 between GPP and CR, and its magnitude was relatively small compared to GPP and
251 CR. Small errors in GPP (or CR) could therefore result in large errors in NCP. Given

252 the fact that there was no pattern in the response of CR to the Kuroshio intrusion (see
253 "Results"), NCP at each station was estimated by subtracting the average CR at all
254 stations from the corresponding GPP at each station.
255
256 **2.5 Size-fractionated respiration derived from *in vitro* INT reduction capacity**
257 **assay**
258 Size-fractionated respiration was estimated based on *in vitro* INT reduction rates
259 as described by *Martínez‐García et al.* [2009]. The sampling depths were the same
260 as the depths sampled for the *in vitro* oxygen-based microbial metabolism
261 measurements. Four 200-ml polypropylene plastic bottles were filled with seawater.
262 One bottle was immediately fixed by adding formaldehyde (2% w/v final
263 concentration) as a blank. Fifteen minutes later, the four replicates were inoculated in
264 the dark by the addition of 2-(ρ-iodophenyl)-3- (ρ-nitrophenyl)-5phenyl tetrazolium
265 chloride salt (INT, Sigma, USA) at a final concentration of 0.8 mM. The INT samples
266 were incubated at the same temperature as the dissolved oxygen bottles. After
267 incubations of 2–3 h, the reactions were stopped by adding formaldehyde. All the
268 samples were sequentially filtered after 15 min through 0.8 and 0.2 μm pore size
269 polycarbonate filters and stored frozen until further processing. The INT_f reduction
270 rates were measured using a SP-8001 UV/Vis Spectrophotometer at 485 nm following
271 the procedure of *Martínez‐García et al.* [2009].

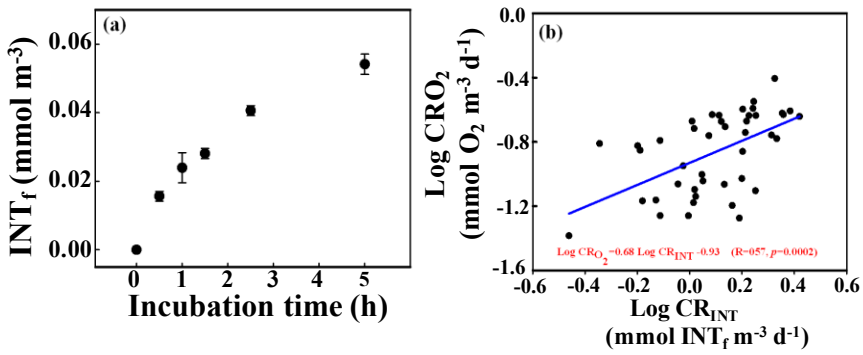

Figure 2. (a) The relationship between rates of INT_f (formazan) reductions and incubation time from a depth of 5 m at SEATS station (b) pair measurements of log-transformed community respiration derived from rates of 2–4-h *in vitro* INT reductions and 24-h rates of oxygen consumption. The blue line represents the linear relationship derived from the paired measurements of log-transformed community respiration.

A time-course experiment was conducted during the same research cruise at the surface at the SEATS station. The optimal incubation time was found to be <4 h (Figure 2a). Therefore, all our incubations were undertaken for <4 h. INT reduction rates were converted to oxygen units using the linear relationship: Log CR_{O2}= 0.68 Log CR_{INT} −0.93 (r = 0.57, p = 0.002) derived from comparisons of paired measurements of CR_{INT} and CR_{O2} (Figure 2b). Bacterial respiration (BR) was defined as the respiration contributed by the 0.2–0.8 μm size fraction [*García-Martín et al.*, 2017].

2.6 Bacterial production

Bacterial production (BP) was estimated using the ^{3}H-leucine incorporation methods of *Kirchman* [1993]. Four 1.8-mL aliquots of water from each depth were

291 incubated with a saturating concentration (10 nmol L−1) of ^{3}H-leucine (Perkin Elmer,
292 USA) for 2 h in the dark. One sample was immediately killed by adding 100%
293 trichloroacetic acid (TCA) as a control, and the other three reactions were terminated
294 with TCA at the end of the incubation. The samples were filtered onto 0.2 μm
295 polycarbonate filters (GE Water & Process Technologies). The filters were washed
296 twice with 3 mL 5% TCA and twice with 2 mL 80% ethanol before being frozen
297 at −20 °C. Upon return to the lab, radioactivity retained on the samples was measured
298 as disintegrations per minute using a Tri-Carb 2800TR liquid scintillation counter
299 (Perkin Elmer, USA). To convert the incorporation of leucine to carbon units, we used
300 a factor of 1.5 kg C mol leucine^{-1}, assuming no isotopic dilution. Bacterial growth
301 efficiency (BGE) was equated to BP/(BR + BP). BR was converted to a carbon basis
302 using a respiratory quotient of 0.9 for calculation of BGE [*Hedges et al.*, 2002; *Laws*,
303 1991].
304
305 **2.7 Estimates of the amount of inorganic nitrogen released by bacterial**
306 **catabolism at ~60% Kuroshio water**
307 Bacteria utilize organic matter in two ways: some of the organic matter is
308 incorporated into bacterial biomass; the remainder is catabolized and released back
309 into the seawater in inorganic form. The total bacterial demand for organic matter is
310 the sum of the amount of organic matter assimilated into bacterial biomass and

311 respired. Our measured BGE, which was derived from the ratio of carbon-based BP to
312 the total bacterial carbon demand, was a metric of the efficiency of organic carbon
313 utilization by the bacteria. The total bacterial nitrogen demand can likewise be
314 expressed as the sum of the bacterial biomass nitrogen (BB_N) requirement and the
315 amount of nitrogen remineralized via bacterial catabolism (BC_N). Based on the i*n situ*
316 observations of bacterial abundance and BGE in terms of carbon utilization, we could
317 roughly estimate the amount of BC_N by the empirical nitrogen content of bacterial
318 biomass and assuming the bacterial nitrogen regeneration efficiency is similar with
319 the carbon regeneration efficiency. If we hypothesize that our observed elevation of
320 inorganic nitrogen concentration (NH_4^++NO_3^-) in 60% Kuroshio water was due
321 mainly to bacterial decomposition of DON from the Kuroshio (see "Discussion"), we
322 would expect that the BC_N would be quantitatively consistent with the observed
323 increase of the inorganic nitrogen concentration in the seawater. There is no a priori
324 reason, however, that the BGEs are the same for carbon and nitrogen, particularly if
325 the C:N ratios of the substrate and bacterial biomass differ. Goldman *et al*. [1987], for
326 example, have reported that the BGE is higher (lower) for carbon than for nitrogen if
327 the C:N ratio of the substrate is lower (higher) than the C:N ratio of the bacterial
328 biomass. Because we had no information on the C:N ratio of the dissolved organic
329 matter used by the bacteria, we assumed the BGEs to be the same for carbon and
330 nitrogen.

To account for the effect of mixing on the two water masses, we first calculated what the concentrations of bacteria and inorganic nitrogen would be in the absence of any sources or sinks (Table 2). For example, the theoretical bacterial abundance at R_K = 60% was estimated to be 40% of the bacterial abundance at $R_K = 0$ plus 60% of the bacterial abundance at $R_K = 100\%$. The values corresponding to $R_K = 0$ and $R_K = 60\%$ were derived from the intercepts of the linear regressions in Figures 3 and 4 to $R_K =$ 0% and $R_K = 100\%$. The anomaly of bacterial nitrogen biomass ($\mathbf{\Delta}BB_N$) was equated to the anomaly of bacterial abundance multiplied by the product of the empirical bacterial carbon content (20 fg C $cell^{-1}$) [Fukuda et al., 1998] and the N:C elemental ratio (1:5) for marine bacteria reported by Goldman *et al*., [1987]. Then BC_N was equated to the difference between $\mathbf{\Delta}BB_N$/BGE and $\mathbf{\Delta}BB_N$. The BGE here was assumed to be 20–24% based on our *in situ* measurement near $R_K = 60\%$ (see "Results" and Figure 8f). We compared the calculated BC_N to the anomaly of the *in situ* $NH_4^+ + NO_3^-$ concentration in the seawater, which was equated to the difference between the measured $NH_4^+ + NO_3^-$ concentration and the theoretical value calculated from mixing of the two endpoint concentrations at $R_K = 0$ and $R_K = 60\%$.

2.8 Statistical analysis

Areal rates within the euphotic zone were calculated by trapezoidal integration of the volumetric data from the surface down to the depth of 1% incident irradiance. The standard errors for integrated values were estimated by propagating the errors of the

independent measurements in accord with *Miller and Miller* [1988]. The data (except for NCP because some NCPs were negative) were log-transformed to satisfy the assumption of normality, which was examined (after transformation) via a Kolmogrov–Smirnov test. Many of the measured variables (i.e., nitrate, BA, GPP, and BGE) were unimodal functions of R_K and passed through a maximum at intermediate R_K values (see "Results"). The implication is that there was a "source" between the two endpoints at $R_K = 0\%$ and $R_K = 100\%$. In other words, if there were no source or sink of these variables, all the data would lie on a straight line between the end points. Equation 3 assumes this to be the case for salinity. We therefore hypothesized that there existed an optimum fraction (R_{Kopt}) of Kuroshio water that corresponded to the maxima of these variables and that these maxima reflected admixture of Kuroshio water containing an essential factor lacking in NSCS water with NSCS water containing another essential factor lacking in Kuroshio water. To test this hypotheses, the variables were first divided into two groups of R_K values higher than and lower than an assumed intermediate value of R_K, and the two sets of variables were fit separately to straight lines with a common intercept, which we equated to R_{Kopt}. The first line was used to describe the tendency of the metrics with R_K less than R_{Kopt}, and the second line was used to describe the data with R_K greater than R_{Kopt}. The statistical significance of this piecewise linear function was determined by comparing the difference between the sum of the squared deviations of the piecewise linear function from the data to the right and left of R_{Kopt} and the sum of the squared

deviations of a horizontal line through the mean of all data with the sum of the squared deviations from the regression lines using an F test with 2 and N – 3 degrees of freedom, where N is the total number of data points, and 3 is the number of adjustable parameters (one intercept and two slopes) in the piecewise linear model. The type I error rate (p value) associated with this F statistic was determined using R software [*Core*, 2014]. The division of two subset was conducted under the condition that piecewise linear function gave the best fit to the data (lowest type I error rate, i.e., the sum of the squared deviations of the data from the piecewise linear function was as small as possible, Table 1). The relationship was judged to be significant if the type I error rate (p) was less than 0.05. Figures 1 and 3 were plotted by software Ocean Data View [*Schlitzer*, 2012]. The complete dataset is available in the supporting information and has also been deposited in the public global respiration database: https://www.uea.ac.uk/environmental-sciences/people/profile/carol-robinson#researchTab (dataset is maintained by Carol Robinson).

3. Results

3.1 Kuroshio intrusion and N-based nutrients

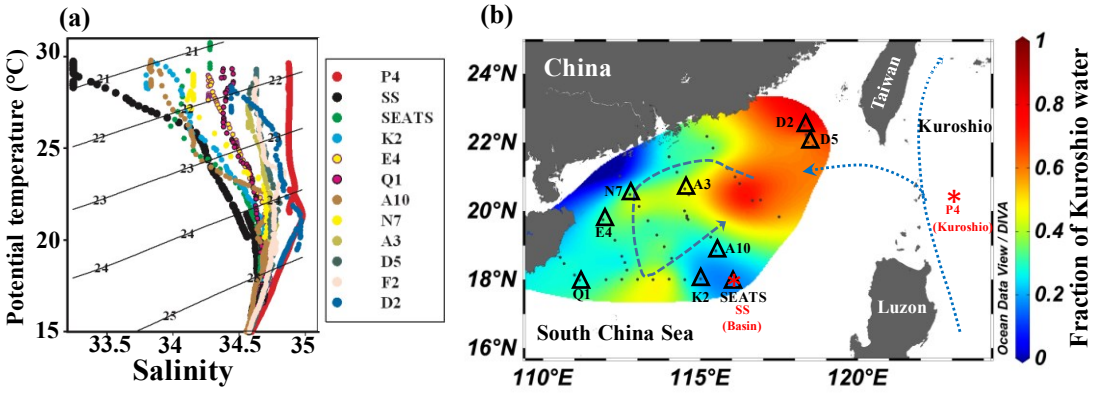

Figure 3. (a) Potential temperature versus salinity at the incubation stations. The black numbers indicate the potential density anomaly (kg m^{-3}). The red and black data indicate typical Kuroshio water (P4) and South China Sea water (SS), which were selected as the two end members for the isopycnal mixing model according to *Du et al.* [2013]. (b) The average fractions of Kuroshio water (upper 100 m) in the NSCS during the cruise. The triangles indicate the station with incubation experiment.

A full description of the Kuroshio intrusion and nutrient concentrations during the sampling period has been reported in *Xu et al.* [2018]. As seen from the T-S diagram (θ-S) in Figure 3a, the hydrologic characterization of incubation stations indicated a mixture of NSCS and Kuroshio water, and all the data points fell within limits defined by the two representative end members: SCS water (SS) and Kuroshio water (P4). At potential density anomalies (σ_θ) < 25.8 kg m^{-3}, the Kuroshio water tended to show higher potential temperature and salinity than the NSCS water on the same isopycnal (Figure 3a). The contour plot showed a clear pathway of Kuroshio intrusion into the NSCS basin via the Luzon Strait, with a higher fraction of Kuroshio water near the eastern and northern part of the basin (Figure 3b). At our incubation stations, the estimated R_K in the upper 100 m obtained from the two-member model

varied between 0.17 at station SEATS and 0.79 at station D2 (Figure 3b).

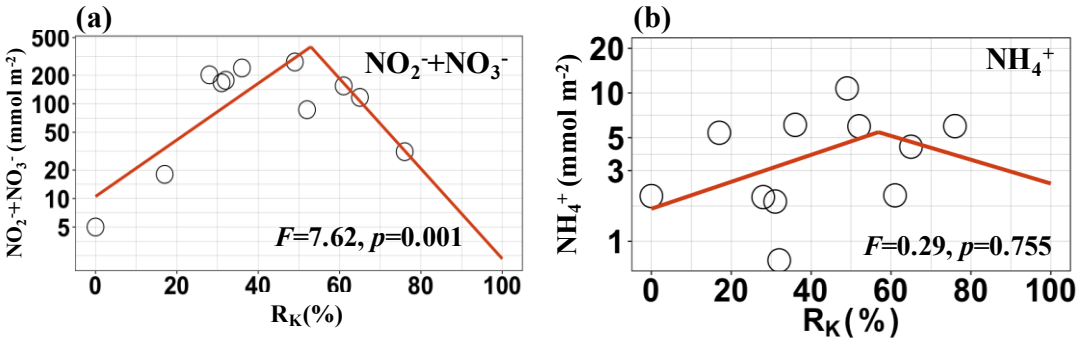

Figure 4. (a) Integrated NO_3^- concentration (b) integrated NH_4^+ versus the fraction of Kuroshio intrusion in the upper 100m (R_K). The NH_4^+ and NO_3^- data were compiled from *Xu et al.* [2018]. The data on the ordinate are plotted on a logarithmic scale. The *F* and *p* represent the *F* statistic and its associated type I error rate, respectively.

The integrated NO_3^- concentration within the upper 100 m ranged between 5 mmol m^{-2} and 276 mmol m^{-2} (Figure 4a). The integrated NO_3^- concentration reached a maximum at an R_K of ~50% (Figure 4a). The statistical analysis indicated that the piecewise linear model was a significant improvement over a horizontal line in describing the data ($F = 7.62$, $p = 0.001$, Table 1, Figure 4a). The integrated NH_4^+ concentrations were one order magnitude lower than the integrated NO_3^- concentrations and varied between 0.77 mmol m^{-2} and 10.7 mmol m^{-2} (Figure 4b). The peak value of the integrated NH_4^+ concentrations was coincident with the maximum of the integrated NO_3^- concentrations at an R_K of 50%, but the piecewise linear model was not a significant improvement over a horizontal line in describing the data ($F = 0.29$, p=0.755, Table 1, Figure 4b).

3.2 Phytoplankton community structure and bacterial abundance

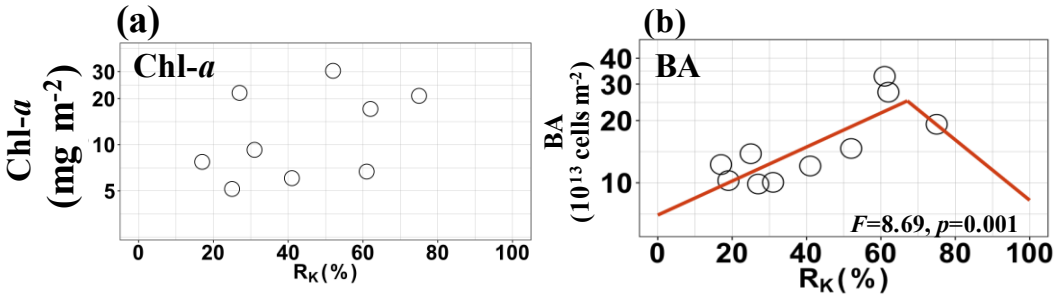

Figure 5. (a) Integrated Chlorophyll-*a* (Chl-*a*) concentration and (b) integrated bacterial abundance (BA) versus the fraction of Kuroshio intrusion in the upper 100m (R_K). The data on the ordinate are plotted on a logarithmic scale. The *F* and *p* represent the *F* statistic and its associated type I error rate, respectively.

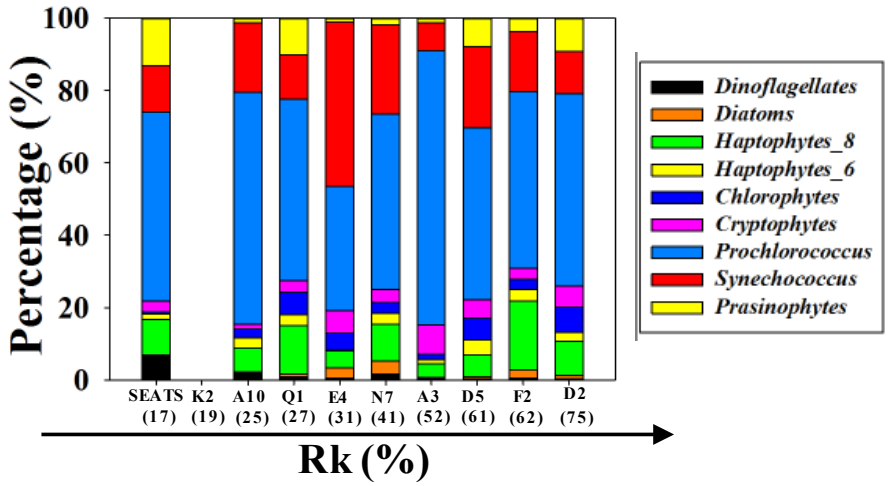

Figure 6. The contributions of different phytoplankton groups to the total integrated Chl-*a* concentration in the euphotic zone. The numbers in the bracket indicate the fraction of Kuroshio intrusion in the upper 100 m (R_K). The sample for HPLC analysis at station K2 was missing.

The integrated Chl-*a* concentrations at our sampling stations were relatively low and ranged from 5.14 to 30.4 mg m^{-2} (Figure 5a). There was no clear relationship between the integrated Chl-*a* and R_K (Figure 5a). The pigment data revealed that all

443 the incubation stations were dominated by *Prochlorococcus* and *Synechococcus*,
444 which are small cyanobacteria (Figure 6). These two genera accounted for most of the
445 Chl-*a* (~72%). Haptophytes_8 and Haptophyts_6 together accounted for ~16% of the
446 Chl-*a*. The biomass of these dominant groups was not significantly affected by the
447 intrusion of Kuroshio Current water (Figure 6). The integrated bacterial abundance
448 reached a peak of 3.3×10^{14} cells m^{-2} at an R_K of ~65% (Figure 5b), and the
449 piecewise linear model (Figure 5b) gave a much better fit to the data than a horizontal
450 line. ($F = 8.69$, p=0.001, Table 1, Figure 5b).

451

452 **Table 1.** Statistical analysis of goodness of fit of piecewise linear model to euphotic
453 zone–integrated variables versus the fraction of Kuroshio water (R_K). The *F* statistic
454 was used to judge whether the piecewise linear model was a significant improvement
455 over a horizontal line in describing the data. Significant effects are in bold (p<0.05).
456 R_{opt} is the value of R_K corresponding to the maximum of the piecewise linear
457 function.

Variable	R_{opt} (%)	*F ratio*	Significance (*p*)
NH_4^+	56	0.29	0.755
NO_3^-	**52**	**7.62**	**0.001**
Chlorophyll *a*	-	-	-
Bacterial abundance	**67**	**8.69**	**0.001**
Gross primary production	**53**	**16**	**0.02**
Community respiration (O_2)	61	2.7	0.078
Net community production	**53**	**10.3**	**0.008**
Bacterial production	**59**	**6.54**	**0.003**
Bacterial respiration	51	1.3	0.320
Bacterial growth efficiency	**66**	**3.9**	**0.042**

458

459

460 **3.3 Euphotic-zone integrated microbial responses to the Kuroshio intrusion**

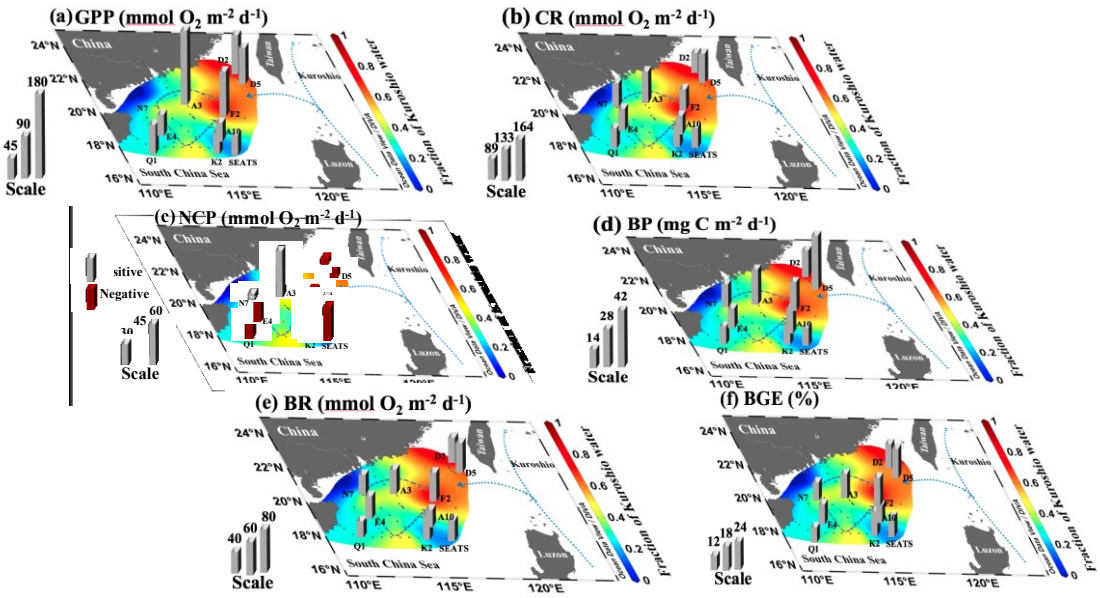

Figure 7. Spatial distributions of the integrated (a) gross primary production (GPP), (b) community respiration (CR), (c) net community production (NCP), (d) bacterial production (BP), (e) bacterial respiration (BR), and (f) bacterial growth efficiency (BGE) within the euphotic zone in the northern South China Sea during the cruise.

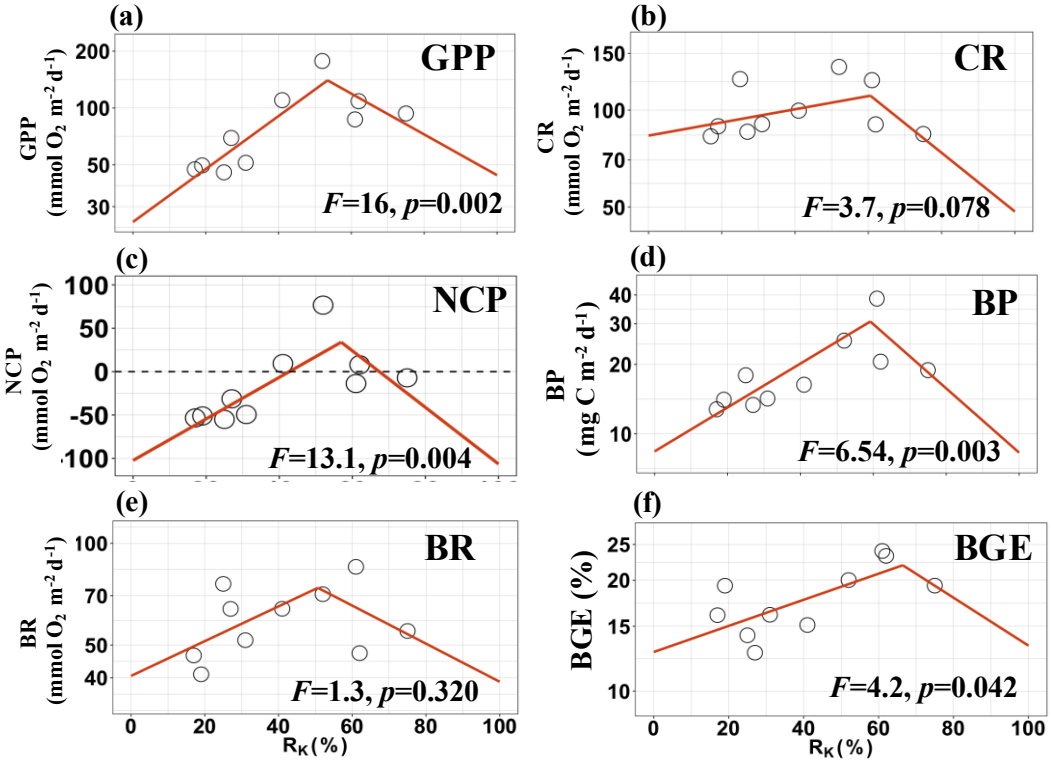

Figure 8. The relationships between the integrated metabolic rates versus the fraction of Kuroshio intrusion in the upper 100 m (R_K). The *F* and *p* represent the *F* statistic

and its associated type I error rate, respectively. The data on the ordinate are plotted on a logarithmic scale (except for NCP). GPP: gross primary production; CR: community respiration; NCP: net community production; BP: bacterial production; BR: bacterial respiration; BGE: bacterial growth efficiency.

Figures 7 and Figure 8 show the spatial distributions of integrated microbial metabolism within the euphotic zone and their relationships with R_K. For oxygen-based metabolism, the integrated GPP and NCP exhibited more pronounced spatial variability (Figure 7a and 7c). The GPPs varied between 45.6 mmol O_2 m^{-2} d^{-1} at station A10 and 177 mmol O_2 m^{-2} d^{-1} at station A3 (Figure 7a). The graph of GPP versus R_K revealed a unimodal relationship between GPP and R_K, with a maximum GPP at an R_K of about 50% (Figure 8a). Because the NCP was derived from the GPP subtracted by constant CR, the spatial pattern of the integrated NCP was similar to that of GPP (Figure 7c). The NCPs were positive at R_K values of 40–80% with the maximum (76.6 mmol O_2 m^{-2} d^{-1}) observed at R_K=52% (Figure 8a and 8c). In the region where R_K was less than 50%, the NCP tended to be negative (Figure 7c and 8c). The piecewise linear model was a significant improvement over a horizontal line in both cases (p =0.008). The spatial distribution of CR was less variable than that of GPP; its mean value was 100 mmol O_2 m^{-2} d^{-1} (Figure 7b). The piecewise linear model did not provide a significantly better description of the CR data than a horizontal line (F = 3.7, p = 0.078, Figure 8b, Table 1).

The integrated BP was positively correlated with R_K from 12.8 mg C m^{-2} d^{-1} at an R_K of 17% (station SEATS) to a peak value of 38.6 mg C m^{-2} d^{-1} at an R_K of 60%

494 (station D5, Figure 7d and 8d). The two BPs at higher R_K values were both less than
495 25 mg C m^{-2} d^{-1} (Figure 8d). The piecewise linear model (Figure8d) gave a much
496 better fit to the BP data than a horizontal line (F=6.54, p=0.003, Table 1). The BR
497 determined by INT reduction rates contributed 30–60% of community respiration on
498 average, with a range of 41.0–85.4 mmol O_2 m^{-3} d^{-1} (Figure 7e). The spatial
499 distribution of BR was relatively homogenous (Figure 7e), and a piecewise linear
500 model did not provide a better description than a horizontal line (F = 1.3, p = 0.320,
501 Table 1, Figure 8e). The calculated BGE varied between 12% and 24% (Figure 8f).
502 The maximum of BP at an R_K of ~60% and the relatively constant BR resulted in the
503 highest BGEs (20–24%) at an R_K of ~60% (Figure 8f). The piecewise linear model
504 was an improvement over a horizontal line at p = 0.042 (Table 1).

505

506 **3.4 The estimated amount of nitrogen released by the bacterial catabolism and**
507 **the peak of inorganic nitrogen concentration in the seawater at R_K = 60%**

508 **Table 2.** Estimates in the anomaly of bacterial nitrogen-based biomass and inorganic
509 nitrogen concentration in the seawater at R_K = 60%. The bacterial nitrogen biomass
510 (BB_N) was estimated from the bacterial abundance (BA) multiplied by the empirical
511 bacterial carbon content (20 fg C $cell^{-1}$) [Fukuda *et al*., 1998] and the atomic N:C
512 elemental ratio (1:5) for bacteria [Goldman *et al*., 1987]. BC_N: the estimated amount
513 of nitrogen released by bacterial catabolism.

514

Variable	R_K=0% (NSCS)	R_K=100% (Kuroshio)	R_K=60% (Theoretical estimates)	R_K=60% (*in situ* measurement)	Anomaly at R_K=60% (Δ)

BA (10^{13} cells m^{-2})	6.6	8.1	7.5	32.4	24.9
BB_N (mmol N m^{-2})	22	27	25	108	83
NH_4^++NO_3^- (mmol N m^{-2})	10.2	5.0	7.1	276	269
BC_N (mmol N m^{-2})	-	-	-	-	249–332

Table 2 shows the anomaly of bacterial nitrogen-based biomass, inorganic nitrogen concentration (NH_4^++NO_3^-), and the estimated amount of nitrogen released by the bacterial catabolism at R_K = 60%. The extrapolated values of BA and inorganic nitrogen at R_K = 0% and 100% (Table 2, Figures 3 and 4) indicated that the Kuroshio (R_K = 100%) had higher bacterial abundance but a lower NH_4^++NO_3^- concentration than the NSCS (R_K = 0%). At R_K = 60%, the anomalies of BA, BB_N, and NH_4^++NO_3^- were 2.49×10^{14} cells m^{-2}, 108 mmol N m^{-2}, and 276 mmol N m^{-2}, respectively (Table 2). Our estimates of BGE (20–24% at R_K = 60%) imply that bacterial catabolism could release 249–332 mmol N m^{-2} (Table 2 and Figure 8f).

4. Discussion

4.1 Quantification of Kuroshio intrusion

Detailed information about the Kuroshio intrusion during the time of our sampling has been provided by *Xu et al.* [2018]. Overall, the Kuroshio water invaded into the

530 NSCS basin from the east to the west through the Luzon Strait (Figure 2b). The
531 hydrographic features of our sampling stations, all of which fell within the θ-S
532 boundaries of the two reference stations (Figure 3a), were consistent with our
533 selection of these two endmembers to calculate R_K values. In this mixing model, we
534 assumed the effects of diapycnal mixing to be negligible compared to isopycnal
535 mixing. *Du et al.* [2013] have used Ca^{2+} as a conservative tracer to validate the model
536 and found that the results predicted from the mixing model agreed well with field
537 observations of Ca^{2+} concentrations in the upper 100 m of the NSCS basin. The
538 threefold higher estimates of nutrient and total organic carbon fluxes from isopycnal
539 mixing compared to diapycnal mixing further support the dominant role of isopycnal
540 mixing [*Du et al.*, 2013; *Wu et al.*, 2015]. In this study, a clearly unimodal pattern of
541 metabolic rates versus R_K was observed, with the maximum of metabolic rates
542 occurring at an R_K of 0.5 or 0.6 (Figure 8 and Figure 9). The significant monotonic
543 decrease of metabolic rates, with the exception of BR and CR, on both sides of the
544 optimum R_K (Figure 8 and Table 1) confirmed our hypothesis that there was an
545 "optimum R_K" for enhancement of microbial metabolism. However, the "optimum
546 R_K" differed between autotrophs and heterotrophs. The optimum R_K was 50% for
547 autotrophic metabolism (i.e., GPP and NCP) and 60% for heterotrophic bacterial
548 variables (i.e., BA, BP, and BGE, Figure 8, Table 1). The mechanism responsible for
549 the "optimum R_K" of these metrics presumably reflects the best combination of DOM
550 (from the Kuroshio) and inorganic nutrients (from the NSCS) in the case of the

heterotrophic bacteria versus inorganic nutrients (from the NSCS and from remineralization of DOM) in the case of the autotrophic community (see the following discussion). The different "optimum R_K" values for the different parameters is also related to the sensitivity and limit of detection of our incubation methodology to quantify the effects of the Kuroshio intrusion on metabolic rates. However, it is worth noting that because the R_K estimated from the two-endmember mixing model is a function of the endmembers, the R_K would not necessarily indicate the absolute contribution of Kuroshio water. Strictly speaking, the R_K that we calculated indicated the relative contribution of water from station P4 (Figure 3), which is located in the main path of the Kuroshio Current (so-call "typical Kuroshio"). The calculated Kuroshio contribution would have increased had we chosen a NSCS station farther to the south with more distinctive hydrography for the NSCS endmember. Therefore, the "optimum R_K" observed in our present study is still a statistical tool that facilitates describing the relative contribution of Kuroshio Current water and enables comparisons of the responses of different variables. Further study is clearly needed to interpret the Kuroshio signal in a more meaningful way, especially for purposes of tracking DOM composition along the pathway of the Kuroshio intrusion.

Despite the fact that some of our incubation stations were closer to land than others, the cyclonic circulation induced by the northeast monsoon effectively isolated the influence of land runoff (Figure 1), and hence our study region was oligotrophic. Similar to major oligotrophic basins, all of our sampling stations were characterized

572 by community structures dominated by pico-phytoplankton and low nitrate
573 concentrations in the upper water column (Figure 6). Hence we were able to examine
574 the effects of the intrusion of Kuroshio water in the absence of other sources of
575 horizontal variability. In the following paragraph, we discuss the impact of the
576 intrusion of the Kuroshio Current on autotrophic and heterotrophic microbial
577 production and microbial community composition.

578

579 **4.2 Response of heterotrophic bacteria**

580 We observed a significant increase of bacterial growth and activity, reflected by
581 higher bacterial abundance (Figure 5a) as well as BP (Figure 7d) at R_K= ~60%. A
582 previous study has also reported a high abundance of heterotrophic bacteria
583 in the Kuroshio-affected region of the NSCS [*Li et al.*, 2017]. The statistical
584 significance of the fit of the piecewise liner model to the data in the cases of BA, BP,
585 and BGE (Figures 5b, 8d, and 8f, respectively) suggests that the Kuroshio and NSCS
586 stimulated bacterial production in a complementary manner. The factors contributing
587 to the enhancement of bacterial activity may have been complex. On the one hand, the
588 enhancement of bacterial metabolism may have resulted from the stimulation of
589 primary production, which is commonly considered to be the main source of organic
590 carbon for bacteria [*Hoppe et al.*, 2002; *Morán et al.*, 2002]. If that were the case, we
591 would have expected a good correlation between the GPP and BP. The weak

relationship between the two variables ($r = 0.38$, $p = 0.268$) suggests that factors other than GPP contributed to the stimulation of BP. Parallel with the maximum value of bacterial metrics at $R_K = 60\%$, there was a similar pattern of NO_3^- concentrations versus R_K with a maximum at $R_K = 50\%$ (Figure 4a). There was no relationship between the integrated NH_4^+ concentrations and R_K (Figure 4 and Figure 8). Ammonium is preferentially taken up by microbes versus nitrate [Pennock and Sharp, 1994] and is thus characterized by a short residence time in seawater. The rapid consumption of NH_4^+ by microbes draws down NH_4^+ concentrations to more-or-less uniformly low levels. Some high NH_4^+ concentrations observed around $R_K = 50–60\%$ (Figure 4) may reflect ammonification of DON and/or excretion by microzooplankton. The peak of inorganic nitrogen at $R_K = 50\%$ is inconsistent with a simple mixing model and implies that there was a source of nitrate (Table 2). Interesting, we found that the estimated amount of inorganic nitrogen (249–332 mmol N m^{-2}) made available by bacterial catabolism was comparable to the difference between the measured areal inorganic nitrogen concentration (276 mmol N m^{-2}) and the areal concentration expected based on simple mixing of Kuroshio and NSCS water (7 mmol N m^{-2}) (Table 2). This similarity indicates that the mechanism that stimulated the bacteria was very likely the DOM transported by the Kuroshio. If this DOM was easily exploited by the specific bacteria in the NSCS, its catabolism could have released inorganic nitrogen into the surrounding water via bacteria-mediated ammonification. The accumulation of DOM in the Kuroshio might have been due to

613 the extremely low inorganic nutrient concentrations in the Kuroshio [*Du et al.*, 2013],
614 which would effectively retard organic matter decomposition [*Carlson et al.*, 2011;
615 *Shiah et al.*, 1998; *Van Wambeke et al.*, 2016]. Nutrient concentrations in the NSCS
616 are relatively high compared to the Kuroshio [*Du et al.*, 2013]. During the mixing of
617 Kuroshio and NSCS water, the former provides DOM, and the latter provides
618 inorganic nutrients. We hypothesize that some bacteria were able to exploit this
619 admixture and, in the process of metabolizing the DOM, released inorganic nitrogen.
620 The DOM in the Kuroshio may therefore be exploited by bacteria that take advantage
621 of the availability of inorganic nutrients provided by the SCS water. This scenario is
622 consistent with the results of two nutrient enrichment experiments conducted in the
623 adjacent western Pacific Ocean [*J Liu et al.*, 2014; *Shiah et al.*, 1998]. Those
624 experiments documented an increased rate of DOC decomposition and an increase of
625 bacterial activity after the addition of inorganic nutrients.

626 Unlike the relationship between BP and R_K, BR remained relatively constant
627 across the range of R_K values (Figure 7e and 9c). This constancy of BR is consistent
628 with the earlier empirical analysis by *López-Urrutia and Morán* [2007]. They found a
629 relatively weak or insignificant relationship between BR and organic matter
630 availability in the upper 200 m of the ocean, unlike the relationship between BP and
631 DOC. Under resource-depleted conditions, the energy provided by bacterial
632 metabolism (i.e., respiration) is allocated to satisfy maintenance metabolic costs
633 [*Carlson et al.*, 2007; *P A del Giorgio, and Cole, J.J.* , 1998]. When resources are less

634 limiting, the metabolic energy is allocated more for biomass production, as reflected
635 by the significant elevation of BGE at R_K = ~60% (Figure 9f).
636
637 **4.3 Response of autotrophic metabolism**
638 At stations with R_K <30%, the integrated GPP averaged 53 ± 5.5 mmol O_2 m^{-2} d^{-1}
639 (Figure 7a), very close to the mean value (51 ± 10 mmol O_2 m^{-2} d^{-1}) determined by
640 the same methodology in the NSCS basin during the summer [*Wang et al.*, 2014].
641 Along the path of the Kuroshio intrusion, we observed a response of GPP around R_K =
642 50% followed by responses from heterotrophic bacteria at R_K = 60% (Figure 8). This
643 pattern suggests that the first effect of mixing Kuroshio water with NSCS water was a
644 stimulation of bacterial activity, and subsequently there was a stimulation of
645 phytoplankton activity. The maximum GPP at the "optimum R_K" was almost 4 times
646 the lowest GPP at R_K = 25%. However, the absence of a corresponding relationship
647 both in the case of Chl-*a* and community structure (Figure 5a and 6) implied that the
648 response of autotrophs to the elevated nitrate concentration near R_K = 50% was a
649 dramatic increase in growth rate but very little change in biomass. This raises a
650 question of how phytoplankton biomass and production are controlled in this system.
651 Based on the estimates from the piecewise linear model, the areal nitrate
652 concentrations at NSCS (R_K = 0%) was about 10.5 mmol m^{-2}, roughly twice the
653 amount of nitrate in the Kuroshio (4.5 mmol m^{-2} at R_K = 0%, Figure 4a). These areal

654 concentrations translate to average concentrations of 105 and 45 nM in the euphotic
655 zone, which are small compared to the half-saturation constant for growth of
656 *Thalassiosira pseudonana* (816 nM) estimated by Garside and Glover [1991].
657 Therefore, the growth rates of the phytoplankton populations in both the NSCS and
658 Kuroshio were limited by inorganic nitrogen. The areal concentration of
659 phytoplankton nitrogen can be estimated by multiplying the average areal Chl-*a*
660 concentration (30.4 mg m^{-2}) by an assumed C: Chl-*a* ratio of 50 g g^{-1} [Strickland and
661 Parsons, 1972] and dividing by an assumed C:N ratio of 5.68 g g^{-1} [Redfield, 1958].
662 This calculation gives an areal phytoplankton nitrogen concentration of 268 mg m^{-2}
663 or 19.1 mmoles m^{-2}, which is only 8% of the peak nitrate concentration of 239 mmol
664 m^{-2} (Figure 4a). The implication is that the enhancement of GPP near R_K = 50% was
665 associated with a biomass of phytoplankton that was a small fraction of the biomass
666 that could have been produced from the elevation of inorganic nitrogen. Previous
667 studies in upwelling systems have shown that the abundance of large phytoplankton,
668 particularly diatoms, increases in response to an influx of inorganic nutrients [Landry
669 *et al*., 1997]. Grazing by macrozooplankton has a limited effect on large diatoms in
670 such cases because macrozooplankton have relatively long generation times [Landry
671 *et al*., 1997]. The absence of a response of large phytoplankton to nitrogen enrichment
672 in this study suggests that a nutrient other than nitrogen may have been limiting. A
673 recent study has indicated that phytoplankton production in the South China Sea basin
674 is co-limited by nitrogen and iron based on observations of a diel cycle of

675 phytoplankton nutritional status assayed by a fluorescence signal [Xie *et al*., 2018].
676 The iron concentration in the upper layer of the NSCS basin during the summer is
677 about 0.2–0.3 nM [Wu *et al*., 2003], which is low enough to lead to iron stress for
678 phytoplankton [Sedwick *et al*., 2000]. The Kuroshio is an extension of the North
679 Equatorial Current (NEC), where iron is limiting [Behrenfeld *et al*., 1996]. Although
680 there has been no report to date of iron concentrations in the subtropical Kuroshio
681 Current, it is reasonable to infer that the iron concentration might be lower in the
682 Kuroshio than in the NSCS because it is an extension of the NEC and is farther from
683 an allochthonous iron source (i.e., Asian dust deposition, Wang *et al*., [2012]) than the
684 NSCS. We hypothesize that low iron concentrations probably limited the growth of
685 large phytoplankton under the nitrate-replete conditions at R_K values near 50%. Small
686 phytoplankton, however, are better able to exploit low iron concentrations because of
687 their relatively large surface-to-volume ratios. Hence their growth rates could increase
688 in response to the increase of nitrate concentrations. However, the microzooplankton
689 that graze *Synechococcus* and *Prochlorococcus* have short generation times and thus
690 can effectively prevent picophytoplankton such as *Synechococcus* and
691 *Prochlorococcus* from increasing in numbers [Landry *et al*., 1997]. The increase in
692 picophytoplankton growth rates at R_K = 50% might thus be counterbalanced by the
693 accompanying increase in the grazing pressure, the result being no change in biomass.
694 Furthermore, increased grazing is associated with an increase in the rate of nutrient
695 recycling, which in turn sustains the rapid growth rate of the picophytoplankton.

696

697 **4.4 Responses of net community production (NCP)**

698 The simultaneous changes of autotrophic and heterotrophic metabolism with
699 changes of R_K resulted in a significant elevation of NCP at R_K = ~50% (Figure 7c and
700 8c). During the summer, strong stratification in the upper water column minimizes the
701 supply of nutrients from deeper water and hence reduces production in the euphotic
702 zone [*Lee Chen*, 2005; *Ning et al.*, 2004; *Wong et al.*, 2007]. As a result, export
703 production in the NSCS during this period is low [*Cai et al.*, 2015; *Lee Chen*, 2005;
704 *Liu and Chai*, 2009]. NCP usually tends to be negative based on oxygen mass-balance
705 models [*Huang et al.*, 2018], dissolved inorganic carbon budgets [*Chou et al.*, 2006],
706 as well as our present incubation results (Figure 7c). However, NCP near R_K = ~50%
707 was positive (Figure 7c). A positive NCP implies that organic carbon is available for
708 export [*Ducklow and Doney*, 2013]. The Kuroshio intrusion–associated shift of
709 metabolic state emphasizes the impact of currents on microbial metabolism and
710 overall carbon cycling in the oligotrophic waters of the NSCS basin.

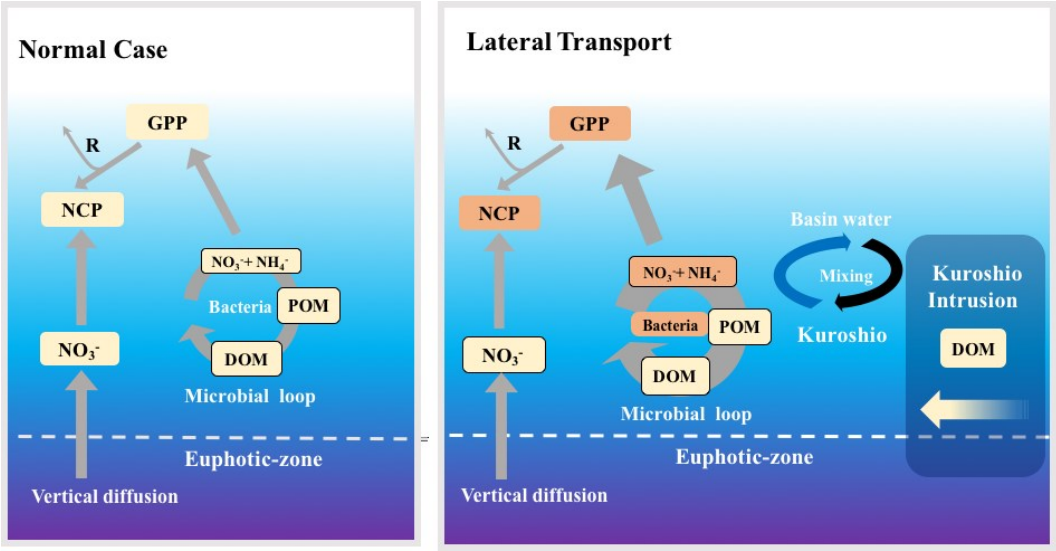

Figure 9. A schematic demonstrating the possible mechanisms responsible for the impacts associated with the intrusion of Kuroshio water on biogeochemical processes in the northern South China Sea basin. DOM: dissolved organic matter. GPP: gross primary production. R: respiration; NCP: net community production; POM: particulate organic matter.

Based on the foregoing results and discussion, we propose a hypothetical mechanism of how transport of Kuroshio water impacts biogeochemical processes in the NSCS basin (Figure 10): Compared to the NSCS, the Kuroshio water is DOM-rich but deficient in inorganic nutrients. We hypothesize that bacterial utilization of DOC in the Kuroshio Current is constrained by the low inorganic nutrient concentrations in the Kuroshio. The intrusion of the Kuroshio into the NSCS basin leads to the admixture of DOC provided by the Kuroshio Current and inorganic nutrients injected by the NSCS. Such mixing processes potentially create a better scenario for some bacteria to exploit and metabolize the DOC. Therefore, the DOC transferred by the Kuroshio intrusion acts as a new carbon source to stimulate the

bacterial activity. The enhanced bacterial activity releases nitrogen during remineralization of DOM. The impact of this newly produced inorganic nitrogen is profound, particularly in a nitrogen-limited ecosystem such as the NSCS basin. On the one hand, the generation of new inorganic nitrogen associated with the Kuroshio intrusion would directly stimulate local phytoplankton primary production and export production by extension. On the other hand, the source of this nitrogen differs from the conventional allochthonous nitrogen that supports export production in the oligotrophic ocean: vertical diffusion [*Du et al.,* 2017], nitrogen fixation [*Karl and Letelier*, 2008], and atmospheric deposition [*Duce et al.*, 2008]. This additional nitrogen is inferred to originate partly from the transfer of organic matter by the Kuroshio Current intrusion and then decomposition into inorganic nitrogen by bacterial activity. Finally, this new nitrogen source will serve as another mechanism to fuel export production and enhance the ability of carbon sequestration in the NSCS basin. This unique mechanism provides more insight into the impact of horizontal currents in the carbon and nitrogen cycle on a regional scale and further broadens our knowledge of the pathways that sustain export production.

5. Conclusion

Overall, the simultaneous responses of autotrophic and heterotrophic activities confirmed the importance of transport of the Kuroshio Current water on microbial

749 community metabolism and biogeochemical processes in the oligotrophic NSCS
750 basin. The statistically negative correlations between the metabolic rates and the
751 absolute value of the deviation of the R_K from the optimum fraction suggests a
752 unimodal impact of the mixture processes in stimulating the microbial metabolism. In
753 other words, there is an “optimum ratio". The observed increase in the nitrogen
754 concentration and export production (net community production in this study) along
755 with the Kuroshio intrusion provided insight into this unique driver of export
756 production in a nutrient-limited system by new nitrogen generated from the intrusion
757 of a current. Our study therefore provides motivation for more accurate quantification
758 of the impact of Kuroshio intrusion on the regional carbon cycle by a combination of
759 a hydrodynamic model and field observations, including seasonal DOC
760 concentrations, nutrient budgets, and export production. Projected climate change
761 scenarios indicate that there will be greater thermal stratification in the upper ocean
762 [*Bopp et al.*, 2013; *Fu et al.*, 2016]. Hence advection will probably become more
763 important relative to vertical mixing in modulating marine biogeochemical processes
764 in the coming decades.

765

766 **Reference**

767 Abell, J., S. Emerson, and P. Renaud (2000), Distributions of TOP, TON and TOC in
768 the North Pacific subtropical gyre: Implications for nutrient supply in the surface
769 ocean and remineralization in the upper thermocline, *Journal of Marine Research*,
770 *58*(2), 203-222, doi:10.1357/002224000321511142.
771 Azam, F., T. Fenchel, J. G. Field, J. S. Gray, L. A. Meyerreil, and F. Thingstad (1983),

772 The ecological role of water-column microbes in the sea, *Marine Ecology*
773 *Progress Series*, *10*(3), 257-263, doi:10.3354/meps010257.
774 Bopp, L., L. Resplandy, J. C. Orr, and S. C. Doney (2013), Multiple stressors of ocean
775 ecosystems in the 21st century: projections with CMIP5 models, *Biogeosciences*,
776 *10*(10), 6225-6245, doi:10.5194/bg-10-6225-2013.
777 Behrenfeld, M. J., A. J. Bale, Z. S. Kolber, J. Aiken, and P. G. Falkowski (1996),
778 Confirmation of iron limitation of phytoplankton photosynthesis in the equatorial
779 Pacific Ocean, Nature, 383(6600), 508-511. doi:10.1038/383508a0
780 Cai, P. H., D. C. Zhao, L. Wang, B. Q. Huang, and M. H. Dai (2015), Role of particle
781 stock and phytoplankton community structure in regulating particulate organic
782 carbon export in a large marginal sea, *Journal of Geophysical Research-Oceans*,
783 *120*(3), 2063-2095, doi:10.1002/2014jc010432.
784 Carlson, C. A., P. A. D. Giorgio, and G. J. Herndl (2007), Microbes and the
785 dissipation of energy and respiration: From cells to ecosystems, *Oceanography*,
786 *20*(2), 89, doi:10.5670/oceanog.2007.52.
787 Carlson, C. A., D. A. Hansell, and C. Tamburini (2011), *DOC persistence and its fate*
788 *After Export Within the Ocean Interior*, 57-59 pp., AAAS, Washington, DC,
789 Microbial Carbon Pump in the Ocean eds Jiao N, Azam F, Sanders S , pp 57–59.
790 Chou, W.C., Y.L. L. Chen, D. D. Sheu, Y.-Y. Shih, C.-A. Han, C. L. Cho, C.-M.
791 Tseng, and Y.-J. Yang (2006), Estimated net community production during the
792 summertime at the SEATS time-series study site, northern South China Sea:
793 Implications for nitrogen fixation, *Geophysical Research Letters*, *33*(22), L22610,
794 doi:10.1029/2005gl025365.
795 Core, T. R. (2014), A language and environment for statistical computing, R
796 foundation for statistical computing, Vienna, Austria., edited.
797 Dai, M., Z. Cao, X. Guo, W. Zhai, Z. Liu, Z. Yin, Y. Xu, J. Gan, J. Hu, and C. Du
798 (2013), Why are some marginal seas sources of atmospheric CO_2?, *Geophysical*
799 *Research Letters*, *40*(40), 2154-2158, doi:10.1002/grl.50390.
800 del Giorgio, P. A., and Cole, J.J. (1998), Bacterial growth efficiency in natural aquatic
801 systems, *Annual Review of Ecology, Evolution, and Systematics*, *29*(29), 503-541,
802 doi:10.1146/annurev.ecolsys.29.1.503.
803 del Giorgio, P. A., J. J. Cole, and A. Cimbleris (1997), Respiration rates in bacteria
804 exceed phytoplankton production in unproductive aquatic systems, *Nature*,
805 *385*(6612), 148-151, doi:10.1038/385148a0.
806 Du, C., Z. Liu, M. Dai, S. J. Kao, Z. Cao, Y. Zhang, T. Huang, L. Wang, and Y. Li
807 (2013), Impact of the Kuroshio intrusion on the nutrient inventory in the upper
808 northern South China Sea: insights from an isopycnal mixing model,
809 *Biogeosciences*, *10*(10), 6419-6432, doi:10.5194/bg-10-6419-2013.
810 Du, C. J., Z. Y. Liu, S. J. Kao, and M. H. Dai (2017), Diapycnal Fluxes of Nutrients in
811 an Oligotrophic Oceanic Regime: The South China Sea, *Geophysical Research*
812 *Letters*, *44*(22), 11510-11518, doi:10.1002/2017gl074921.
813 Duce, R. A., et al. (2008), Impacts of atmospheric anthropogenic nitrogen on the open

ocean, *Science*, *320*(5878), 893-897, doi:10.1126/science.1150369.
Ducklow, H. W. (1999), The bacterial component of the oceanic euphotic zone, *Fems Microbiology Ecology*, *30*(1), 1-10, doi:10.1111/j.1574-6941.1999.tb00630.x.
Ducklow, H. W., and S. C. Doney (2013), What is the metabolic state of the oligotrophic ocean? A debate, *Annual Review of Marine Science*, *5*(1), 525-533, doi:10.1146/annurev-marine-121211-172331.
Falkowski, P. G., E. A. Laws, R. T. Barber, and J. W. Murray (2003), Phytoplankton and their role in primary, new, and export production, *IFasham M.J.R. (eds) Ocean Biogeochemistry. Global Change — The IGBP Series (closed).Springer, Berlin, Heidelberg*, 99-121, doi:10.1007/978-3-642-55844-3_5.
Fang, G., Y. Wang, Z. Wei, Y. Fang, F. Qiao, and X. Hu (2009), Interocean circulation and heat and freshwater budgets of the South China Sea based on a numerical model, *Dynamics of Atmospheres & Oceans*, *47*(1–3), 55-72, doi:10.1016/j.dynatmoce.2008.09.003.
Fontes, M. L. S., A. Berri, M. Carvalho, A. L. O. Fonseca, R. V. Antônio, and A. S. Freire (2018), Bacterioplankton abundance and biomass stimulated by water masses intrusions over the Southern Brazilian Shelf (between 25°57'S and 29°24'S), *Continental Shelf Research*, *164*, 28-36, doi:10.1016/j.csr.2018.05.003.
Fu, W., J. Randerson, and J. K. Moore (2016), Climate change impacts on net primary production (NPP) and export production (EP) regulated by increasing stratification and phytoplankton community structure in CMIP5 models, *Biogeosciences Discussions*,*12*(15), 12851-12897 doi:10.5194/bgd-12-12851-2015.
Fukuda, R., H. Ogawa, T. Nagata, and I. Koike (1998), Direct determination of carbon and nitrogen contents of natural bacterial assemblages in marine environments, *Applied and Environmental Microbiology*, 64(9), 3352-3358.
Furuya, K., and K. Harada (1995), An automated precise Winkler titration for determining dissolved oxygen on board ship, *Journal of Oceanography*, *51*(3), 375-383, doi:10.1007/bf02285173.
Gan, J., Z. Liu, and C. R. Hui (2016), A Three-Layer Alternating Spinning Circulation in the South China Sea, *Journal of Physical Oceanography*, *46*(8), 2309-2315, doi:10.1175/jpo-d-16-0044.1.
García-Martín, E. E., M. Aranguren-Gassis, M. Hartmann, M. V. Zubkov, and P. Serret (2017), Contribution of bacterial respiration to plankton respiration from 50°N to 44°S in the Atlantic Ocean, *Progress in Oceanography*, *158*, 99-108, doi:10.1016/j.pocean.2016.11.006.
Gist, N., P. Serret, E. M. S. Woodward, K. Chamberlain, and C. Robinson (2009), Seasonal and spatial variability in plankton production and respiration in the Subtropical Gyres of the Atlantic Ocean, *Deep Sea Research Part II: Topical Studies in Oceanography*, *56*(15), 931-940, doi:10.1016/j.dsr2.2008.10.035.
Goldman, J. C., D. A. Caron, and M. R. Dennett (1987), Regulation of gross growth efficiency and ammonium regeneration in bacteria by substrate C:N ratio,

Limnology and Oceanography, *32*(6), 1239-1252. doi: 10.4319/lo.1987.32.6.1239

Gong, G.-C., Y.-H. Wen, B.-W. Wang, and G.-J. Liu (2003), Seasonal variation of chlorophyll *a* concentration, primary production and environmental conditions in the subtropical East China Sea, *Deep Sea Research Part II: Topical Studies in Oceanography*, *50*(6-7), 1219-1236, doi:10.1016/s0967-0645(03)00019-5.

Han, A., M. Dai, S.-J. Kao, J. Gan, Q. Li, L. Wang, W. Zhai, and L. Wang (2012), Nutrient dynamics and biological consumption in a large continental shelf system under the influence of both a river plume and coastal upwelling, *Limnology and Oceanography*, *57*(2), 486-502, doi:10.4319/lo.2012.57.2.0486.

Hedges, J. I., J. A. Baldock, Y. Gélinas, C. Lee, M. L. Peterson, and S. G. Wakeham (2002), The biochemical and elemental compositions of marine plankton: A NMR perspective, *Marine Chemistry*, *78*(1), 47-63, doi:10.1016/S0304-4203(02)00009-9.

Hoppe, H. G., K. Gocke, R. Koppe, and C. Begler (2002), Bacterial growth and primary production along a north-south transect of the Atlantic Ocean, *Nature*, *416*(6877), 168-171, doi:10.1038/416168a.

Hu, D., et al. (2015), Pacific western boundary currents and their roles in climate, *Nature*, *522*(7556), 299-308, doi:10.1038/nature14504.

Hu, J., H. Kawamura, H. Hong, and Y. Qi (2000), A Review on the currents in the South China Sea: seasonal circulation, South China Sea warm current and Kuroshio intrusion, *Journal of Oceanography*, *56*(6), 607-624, doi:10.1023/a:1011117531252.

Huang, Y., B. Chen, B. Huang, H. Zhou, and Y. Yuan (2019), Potential overestimation of community respiration in the western Pacific boundary ocean: What causes the putative net heterotrophy in oligotrophic systems?, *Limnology and Oceanography*, doi:10.1002/lno.11179.

Huang, Y., B. Yang, B. Chen, G. Qiu, H. Wang, and B. Huang (2018), Net community production in the South China Sea Basin estimated from *in situ* O_2 measurements on an Argo profiling float, *Deep Sea Research Part I: Oceanographic Research Papers*, *131*, 54-61, doi:10.1016/j.dsr.2017.11.002.

Huthnance, J. M., J. T. Holt, and S. L. Wakelin (2009), Deep ocean exchange with west- European shelf seas, *Ocean Science*, *5*(4), 621-634, doi:10.5194/os-5-621-2009.

Jenkins, W. J., and S. C. Doney (2003), The subtropical nutrient spiral, *Global Biogeochemical Cycles*, *17*(4), 1110, doi:10.1029/2003GB002085.

Johnson, K. S., S. C. Riser, and D. M. Karl (2010), Nitrate supply from deep to near-surface waters of the North Pacific subtropical gyre, *Nature*, *465*, 1062, doi:10.1038/nature09170.

Karl, D. M., and R. M. Letelier (2008), Nitrogen fixation-enhanced carbon sequestration in low nitrate, low chlorophyll seascapes, *Marine Ecology Progress Series*, *364*, 257-268, doi:10.3354/meps07547.

Kirchman, D. (1993), Leucine incorporation as a measure of biomass production by

heterotrophic bacteria, *Handbook of Methods in Aquatic Microbial Ecology. Lewis*, 509-512,In P. F.Kemp, B. F. Sherr, E. B. Sherr, and J. J. Cole [eds.], Handbookof methods in aquatic microbial ecology. Lewis Publishers.

Laws, E. A. (1991), Photosynthetic quotients, new production and net community production in the open ocean, *Deep Sea Research Part I 38*(1), 143-167, doi:10.1016/0198-0149(91)90059-O.

Lee Chen, Y.-l. (2005), Spatial and seasonal variations of nitrate-based new production and primary production in the South China Sea, *Deep Sea Research Part I: Oceanographic Research Papers*, *52*(2), 319-340, doi:10.1016/j.dsr.2004.11.001.

Lee Chen, Y.-l., and H.-Y. Chen (2006), Seasonal dynamics of primary and new production in the northern South China Sea: The significance of river discharge and nutrient advection, *Deep Sea Research Part I: Oceanographic Research Papers*, *53*(6), 971-986, doi:10.1016/j.dsr.2006.02.005.

Lee Chen, Y.-l., H.-Y. Chen, S.-h. Tuo, and K. Ohki (2008), Seasonal dynamics of new production from Trichodesmium N2 fixation and nitrate uptake in the upstream Kuroshio and South China Sea basin, *Limnology and oceanography*, *53*(5), 1705, doi:10.4319/lo.2008.53.5.1705.

Letscher, R. T., F. Primeau, and J. K. Moore (2016), Nutrient budgets in the subtropical ocean gyres dominated by transport, *Nature Geoscience*, *9*(11), 815-819, doi:10.1038/ngeo2812.

Li, J., X. Jiang, G. Li, Z. Jing, L. Zhou, Z. Ke, and Y. Tan (2017), Distribution of picoplankton in the northeastern South China Sea with special reference to the effects of the Kuroshio intrusion and the associated mesoscale eddies, *Science of the Total Environment 589*, 1-10, doi:10.1016/j.scitotenv.2017.02.208.

Liu, G., and F. Chai (2009), Seasonal and interannual variability of primary and export production in the South China Sea: a three-dimensional physical-biogeochemical model study, *Ices Journal of Marine Science*, *66*(2), 420-431, doi:10.1093/icesjms/fsn219.

Liu, J., N. Jiao, and K. Tang (2014), An experimental study on the effects of nutrient enrichment on organic carbon persistence in the western Pacific oligotrophic gyre, *Biogeosciences*, *11*(18), 5115-5122, doi:10.5194/bg-11-5115-2014.

Liu, K. K., S. Y. Chao, P. T. Shaw, G. C. Gong, C. C. Chen, and T. Y. Tang (2002), Monsoon-forced chlorophyll distribution and primary production in the South China Sea: observations and a numerical study, *Deep Sea Research Part I: Oceanographic Research Papers*, *49*(8), 1387-1412, doi:10.1016/s0967-0637(02)00035-3.

Liu, X., W. Xiao, M. R. Landry, K. P. Chiang, L. Wang, and B. Huang (2016), Responses of phytoplankton communities to environmental variability in the East China Sea, *Ecosystems*, *19*(5), 832-849, doi:10.1007/s10021-016-9970-5.

López-Urrutia, Á., and X. A. G. Morán (2007), Resource limitation of bacterial production distorts the temperature dependence of oceanic carbon cycling, *Ecology*,

940 *88*(4), 817-822, doi:10.1890/06-1641.
941 Lozier, M. S., A. C. Dave, J. B. Palter, L. M. Gerber, and R. T. Barber (2011), On the
942 relationship between stratification and primary productivity in the North
943 Atlantic, *Geophysical Research Letters*, *38*(18), 178-187,
944 doi:10.1029/2011GL049414.
945 Lundry, M. R., et al. (1997), Iron and grazing constraints on primary production in the
946 central equatorial Pacific: An EqPac synthesis, *Limnology and Oceanography*,
947 42(3), 405-418. doi: 10.4319/lo.1997.42.3.0405
948 Mackey, M., D. Mackey, H. Higgins, and S. Wright (1996), CHEMTAX - a program
949 for estimating class abundances from chemical markers:application to HPLC
950 measurements of phytoplankton, *Marine Ecology Progress*, *144*(1), 265-283.
951 Marie, D., F. Partensky, S. Jacquet, and D. Vaulot (1997), Enumeration and cell cycle
952 analysis of natural populations of marine picoplankton by flow cytometry using
953 the nucleic acid stain SYBR Green I, *Applied and Environmental Microbiology*,
954 *63*(1), 186-193.
955 Martínez-García, S., E. Fernández, M. Aranguren-Gassis, and E. Teira (2009), In vivo
956 electron transport system activity: a method to estimate respiration in natural
957 marine microbial planktonic communities, *Limnology & Oceanography Methods*,
958 *7*(5), 626-629, doi:10.4319/lom.2009.7.459
959 Miller, J. C., and J. N. Miller (1988), Statistics for analytical chemistry, 2nd edition,
960 *Analytical and Bioanalytical Chemistry*, *378*(7), Ellis Howood Limtied, Great
961 Britain.
962 Morán, X. A., M. Estrada, J. M. Gasol, and C. Pedrós-Alió (2002), Dissolved primary
963 production and the strength of phytoplankton- bacterioplankton coupling in
964 contrasting marine regions, *Microbial Ecology*, *44*(3), 217-223,
965 doi:10.1007/s00248-002-1026-z.
966 Nan, F., H. Xue, and F. Yu (2015), Kuroshio intrusion into the South China Sea: A
967 review, *Progress in Oceanography*, *137*, 314-333,
968 doi:10.1016/j.pocean.2014.05.012.
969 Ning, X., F. Chai, H. Xue, Y. Cai, C. Liu, and J. Shi (2004), Physical-biological
970 oceanographic coupling influencing phytoplankton and primary production in the
971 South China Sea, *Journal of Geophysical Research: Oceans*, *109*(C10),
972 doi:10.1029/2004JC002365.
973 Oudot, C., R. Gerard, P. Morin, and I. Gningue (1988), Precise shipboard
974 determination of dissolved-oxygen (Winkler procedure) for productivity
975 studies with a commercial system, *Limnology and Oceanography*, *33*(1), 146-
976 150, doi:10.4319/lo.1988.33.1.0146.
977 Patey, M. D., M. J. A. Rijkenberg, P. J. Statham, M. C. Stinchcombe, E. P. Achterberg,
978 and M. Mowlem (2008), Determination of nitrate and phosphate in seawater at
979 nanomolar concentrations, *Trends in Analytical Chemistry*, *27*(2), 169-182,
980 doi:10.1016/j.trac.2007.12.006.
981 Pennock, J. R., and J. H. Sharp (1994), Temporal alteration between light- and

nutrient- limitation of phytoplankton production in a coastal plain estuary, *In: Falkowski P.G., Woodhead A.D., Vivirito K. (eds) Primary Productivity and Biogeochemical Cycles in the Sea. Environmental Science Research*, *43*, doi:10.1007/978-1-4899- 0762-2_62.

Qiu, C., H. Mao, J. Yu, Q. Xie, J. Wu, S. Lian, and Q. Liu (2015), Sea surface cooling in the Northern South China Sea observed using Chinese sea-wing underwater glider measurements, *Deep Sea Research Part I: Oceanographic Research Papers*, *105*, 111-118, doi:10.1016/j.dsr.2015.08.009.

Qu, T., H. Mitsudera, and T. Yamagata (2000), Intrusion of the North Pacific waters into the South China Sea, *Journal of Geophysical Research Oceans*, *105*(C3), 6415-6424, doi:10.1029/1999JC900323.

Redfield, A. C. (1958), The biological control of chemical factors in the environment, *American scientist*, 46(3), 230A-221.

Reynolds, S., C. Mahaffey, V. Roussenov, and R. G. Williams (2014), Evidence for production and transport of dissolved organic phosphorus in the eastern subtropical North Atlantic, *Global Biogeochemical Cycles*, *28*(8), 805-824, doi:10.1002/2013gb004801.

Schlitzer, R. (2012), Ocean data view Available at odv.awi.de. Accessed November 3, 2013, edited.

Sedwick, P. N., G. R. DiTullio, and D. J. Mackey (2000), Iron and manganese in the Ross Sea, Antarctica: Seasonal iron limitation in Antarctic shelf waters, *Journal of Geophysical Research: Oceans*, *105*(C5), 11321-11336. doi: 10.1029/2000jc000256

Shiah, F. K., S. J. Kao, and K. K. Liu (1998), Bacterial production in the western equatorial Pacific: Implications of inorganic nutrient effects on dissolved organic Carbon accumulation and consumption, *Bulletin of Marine Science -Miami-*, *62*(3), 795-808.

Shiozaki, T., S. Takeda, S. Itoh, T. Kodama, X. Liu, F. Hashihama, and K. Furuya (2015), Why is Trichodesmium abundant in the Kuroshio?, *Biogeosciences*, *12*(23), 6931-6943, doi:10.5194/bg-12-6931-2015.

Siegel, D. A., K. O. Buesseler, S. C. Doney, S. F. Sailley, M. J. Behrenfeld, and P. W. Boyd (2014), Global assessment of ocean carbon export by combining satellite observations and food-web models, *Global Biogeochemical Cycles*, *28*(3), 181-196, doi:10.1002/2013GB004743.

Sigman, D. M., and E. A. Boyle (2000), Glacial/interglacial variations in atmospheric carbon dioxide, *Nature*, *407*(6806), 859-869, doi:10.1038/35038000.

Strickland, J. D., and T. R. Parsons (1972), A practical handbook of seawater analysis, Fisheries Resource Board: Ottawa Canada., 167, p. 310.

Tian, J., Q. Yang, and W. Zhao (2009), Enhanced diapycnal mixing in the South China Sea, *Journal of Physical Oceanography*, *39*(12), 3191, doi:10.1175/2009JPO3899.1.

Tseng, C. M., G. T. F. Wong, I. I. Lin, C. R. Wu, and K. K. Liu (2005), A unique

seasonal pattern in phytoplankton biomass in low-latitude waters in the South China Sea, *Geophysical Research Letters*, *32*(8), 487-500, doi:10.1029/2004GL022111

Van Wambeke, F., U. Pfreundt, A. Barani, H. Berthelot, T. Moutin, M. Rodier, W. R. Hess, and S. Bonnet (2016), Heterotrophic bacterial production and metabolic balance during the VAHINE mesocosm experiment in the New Caledonia lagoon, *Biogeosciences 13*(11), 3187-3202, doi:10.5194/bg-13-3187-2016.

Viviani, D. A., and M. J. Church (2017), Decoupling between bacterial production and primary production over multiple time scales in the North Pacific Subtropical Gyre, *Deep Sea Research Part I: Oceanographic Research Papers*, *121*(1), 132-142, doi:10.1016/j.dsr.2017.01.006.

Wang, L., B. Huang, K. P. Chiang, X. Liu, B. Chen, Y. Xie, Y. Xu, J. Hu, and M. Dai (2016), Physical-biological coupling in the western South China Sea: the response of phytoplankton community to a mesoscale cyclonic eddy, *PLoS One*, *11*(4), e0153735, doi:10.1371/journal.pone.0153735.

Wang, N., W. Lin, B. Chen, and B. Huang (2014), Metabolic states of the Taiwan Strait and the northern South China Sea in summer 2012 (In Chinese with English abstract), *Journal of Tropical Oceanography*, *33*(4), 61-68.

Wong, G. T. F., C. M. Tseng, L. S. Wen, and S. W. Chung (2007), Nutrient dynamics and nitrate anomaly at the SEATS station, doi:10.1016/j.dsr2.2007.05.011.

Wu, K., M. Dai, J. Chen, F. Meng, X. Li, Z. Liu, C. Du, and J. Gan (2015), Dissolved organic carbon in the South China Sea and its exchange with the Western Pacific Ocean, *Deep Sea Research Part II: Topical Studies in Oceanography*, *122*, 41-51, doi:10.1016/j.dsr2.2015.06.013.

Xiao, W., L. Wang, E. Laws, Y. Xie, J. Chen, X. Liu, B. Chen, and B. Huang (2018), Realized niches explain spatial gradients in seasonal abundance of phytoplankton groups in the South China Sea, *Progress in Oceanography*, *162*, 223-239, doi:10.1016/j.pocean.2018.03.008.

Xie, Y., E. A. Laws, L. Yang, and B. Huang (2018), Diel Patterns of Variable Fluorescence and Carbon Fixation of Picocyanobacteria Prochlorococcus-Dominated Phytoplankton in the South China Sea Basin, *Frontiers in microbiology*, 9, 1589-1589. doi:10.3389/fmicb.2018.01589

Xu, N., et al. (2018), Enhanced ammonia oxidation caused by kuroshio intrusion in the boundary zone of the northern South China Sea, *Geophysical Research Letters*, *0*(0), doi:10.1029/2018GL077896.

Wang, S.-H., N. C. Hsu, S.-C. Tsay, N.-H. Lin, A. M. Sayer, S.-J. Huang, and W. K. M. Lau (2012), Can Asian dust trigger phytoplankton blooms in the oligotrophic northern South China Sea?, *Geophysical Research Letters*, 39(5). doi:10.1029/2011gl050415

Wu, J., S.-W. Chung, L.-S. Wen, K.-K. Liu, Y.-l. L. Chen, H.-Y. Chen, and D. M. Karl (2003), Dissolved inorganic phosphorus, dissolved iron, and *Trichodesmiumin* the oligotrophic South China Sea, *Global Biogeochemical Cycles*, *17*(1), 8-1- 8-

10. doi: 10.1029/2002gb001924
Zhu, Y., D. Yuan, Y. Huang, J. Ma, and S. Feng (2013), A sensitive flow-batch system for on board determination of ultra-trace ammonium in seawater: Method development and shipboard application, *Analytica Chimica Acta*, *794*(17), 47-54, doi:10.1016/j.aca.2013.08.009.

Acknowledgements

This study was supported by grants from the National Key Research and Development Program of China (No.2016YFA0601201), the China NSF Projects (Nos. 41890803, U1805241), and partially supported by the starter grant from University of Strathclyde (to B. Chen). All of the phytoplankton community structure and metabolic rates data are available in the supporting information and please contact Dr. Huang (bqhuang@xmu. edu.cn) if any questions. And the nutrients concentration data could be acquired from the supporting information of Xu *et al*. [2018] (https://doi.org/10.1029/2018GL077896). We also acknowledged the crew in R/V "Dongfanghong II" at the University of Ocean, China. We would like to thank Dr. Hu JianYu for providing the CTD data. This study also benefited from the discussion with Dr. Xu and Dr. Kao Shuji at Xiamen University.

Supporting Information

- Supporting information S1
- Dataset Table S1

- Dataset Table S2
- Dataset Table S3
- Dataset Table S4
- Dataset Table S5

Conflict of interest

The authors declare no conflict of interests.